DOI: 10.1002/chem.200501334

One-Pot Synthesis and Bioapplication of Amine-Functionalized Magnetite Nanoparticles and Hollow Nanospheres

Leyu Wang,[a, b] Jie Bao,[a] Lun Wang,[b] Fang Zhang,[c] and Yadong Li*[a]

Abstract: To demonstrate their applications in biological and medical fields such as in immunoassays, magnetic separation of cells or proteins, drug or gene delivery, and magnetic resonance imaging, the template-free syntheses of water-soluble and surface functionalized magnetic nanomaterials have become essential and are challenging. Herein, we developed a facile one-pot template-free method for the preparation of amine-functionalized magnetite nanoparticles and hollow nanospheres by using $FeCl_3 \cdot 6H_2O$ as single iron source. These magnetic nanomaterials were characterized by TEM, SEM, XRD, and FTIR technologies. Their magnetic properties were also studied by using a superconducting quantum interference device (SQUID) magnetometer at room temperature. Then the amine-functionalized magnetite nanoparticles were applied to immunoassays and magnetic resonance imaging in live mice.

Keywords: bioapplications · hollow nanospheres · magnetic properties · medicinal chemistry · nanostructures

Introduction

Water solubility and surface functionalization of nanomaterials are crucial for bioapplication.[1] The development a facile method for the preparation of water soluble and functionalized (coupled with amino or carboxylic groups) magnetite nanomaterials, especially for the template-free synthesis of amine-functionalized, hollow magnetite spheres, is still an essential yet challenging step as they have much potential in biological and medical fields, such as the immobilization of proteins, peptides, and enzymes;[2–4] bioseparation;[5,6] immunoassays;[7] drug or gene delivery;[8] magnetic resonance imaging (MRI);[10,11] and so on. With the rapid development of nanostructured materials and nanotechnology in the fields of biotechnology and biomedicine, in recent years, iron oxides (Fe_3O_4 and Fe_2O_3), in particular, have received considerable attention for their strong magnetic properties and low toxicity.[12–15] The outstanding potential of these iron oxide nanoparticles has stimulated extensive development of the synthetic technology. To date, many technologies, such as coprecipitation and microemulsion methods,[16,17] and ultrasound irradiation technology[18] have been applied to produce these magnetic nanoparticles. However, the relatively poor size uniformity and crystallinity of the nanoparticles obtained strongly affect their magnetic properties. Recently, an alternative method has been developed to prepare high-quality magnetic nanoparticles by thermal decomposition of different types of iron precursors, such as iron carbonyls ($[Fe(CO)_5]$),[19] iron triacetylacetonate ($[Fe(acac)_3]$),[20,21] cupferronates ($[Fe(Cup)_3]$),[22] and iron oleates[23] in complex organic solvent. These as-prepared nanoparticles have good shape control, monodispersibility and high crystallinity, which are suitable for various magnetic applications, such as data storage and advanced magnets. However, these monodisperse nanomaterials prepared by thermal decomposition technology are only soluble in nonpolar solvents before surface modification, and this greatly inhibits their applications in biotechnology and biomedicine. Meanwhile, the widespread interest in hollow spheres possessing magnetic properties has not only been driven by their broad applications in bioseparation, immunoassays, and magnetic resonance imaging (MRI), but has also been propelled by their nonparalleled advantages in catalyst carri-

[a] Leyu Wang, J. Bao, Prof. Dr. Y. Li
Department of Chemistry, Tsinghua University
Beijing, 100084 (P. R. China)
Fax: (+86) 10-6278-8765
E-mail: ydli@tsinghua.edu.cn

[b] Leyu Wang, Prof. Lun Wang
Anhui Key Laboratory of Functional Molecular Solids
College of Chemistry and Materials Science
Anhui Normal University, Wuhu, 241000 (P. R. China)

[c] F. Zhang
Haidian Hospital, Beijing (P. R. China)

Supporting information for this article is available on the WWW under http://www.chemeurj.org/ or from the author.

er and drug delivery. For instance, strong magnetism of magnetic hollow spheres facilitates immobilized catalyst separation and recyclization as well as product purification, while their large specific surface area enhances catalytic performance. Some key properties of effective delivery vehicles, such as long-term stability, high loading capacity and site selectivity, which help reduce side effects, lower doses needed and development of new therapies, are to be found in magnetic hollow spheres. However, to the best of our knowledge, there is no report of the template-free preparation of amine-functionalized, hollow magnetite nanospheres to date. In this communication, we report on the development of a facile one-pot method for the direct preparation of amine-functionalized magnetite nanoparticles and hollow nanospheres without templates. With highly magnetic properties and the amino groups on the outer surface of the nanoparticles, we also demonstrated their magnetic separation and concentration implications in immunoassays based on the scheme depicted in Figure 1 and magnetic resonance imaging in live mice.

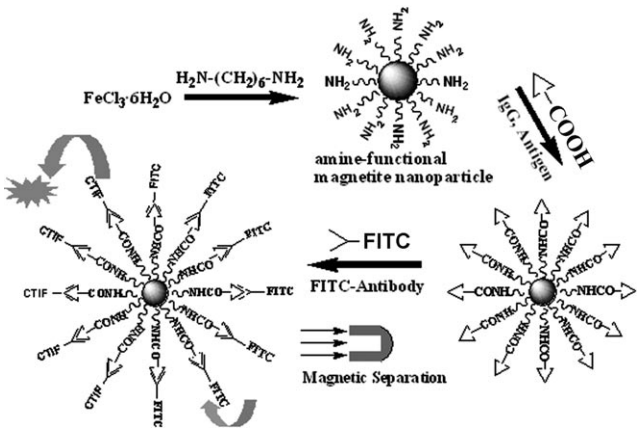

Figure 1. Schematic illustration of the magnetic separation in a fluorescence immunoassay using the amine-functionalized magnetite nanoparticles.

Results and Discussion

By using $FeCl_3{\cdot}6H_2O$ as a single iron source, we prepared the amine-functionalized magnetite nanoparticles with tunable size (from ~15 nm to ~50 nm) and high quality with the 1,6-hexadiamine as the ligand. By controlling the reaction temperature and amount of 1,6-hexadiamine, amine-functionalized, hollow magnetite nanospheres were also produced. In comparison with the previously prepared hydrophilic magnetite microspheres,[24] the as-synthesized high-quality magnetite nanoparticles in this work are more suitable for bioapplication as their size is more appropriate. Second, the magnetic nanocrystals are functionalized with amino groups in the facile one-pot synthetic process, which makes them water soluble and able to bioconjugate with biological macromolecules, such as proteins, peptides, and nucleic acids, and cuts short the complicated and time-consuming procedure for the functional modification of the surface for biological applications. So, the amino groups on the outer surface of the magnetic nanocrystals make them convenient for use in biological and biomedical applications. Last, it is worth noting that the template-free-prepared, amine-functionalized, hollow magnetite nanospheres will find great potentials in catalysis and targeted drug delivery owing to their high magnetization and hollow core; the hollow cores could be used for the carrying of catalyst or drug, and the magnetization would simplify the separation of the catalyst and target the drug delivery.

In this work, the size and morphology of the nanoparticles were observed by TEM images. Figure 2 shows the typical

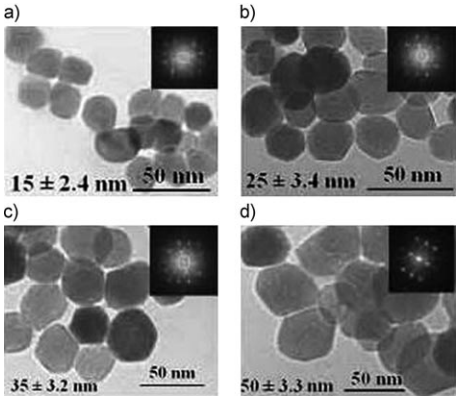

Figure 2. TEM images of the magnetic nanoparticles with different sizes.

TEM images of the as-prepared magnetite nanomaterials; the electron-diffraction patterns revealed the single-crystal nature of these nanocrystals. These images revealed that the magnetic nanomaterials had good dispersibility and high crystallinity. From these images, it can be seen that the average particle size can be easily tuned from ~15 nm up to ~50 nm.

The morphology and crystallography of the as-prepared hollow nanospheres were characterized by SEM, while the hollow structure was clearly revealed by TEM images and SEM images of partly broken, hollow Fe_3O_4 nanospheres. Figure 3a shows that hollow Fe_3O_4 spheres are round in shape and have a fine exterior surface, while contrast between the brightness of central areas and the darkness of the periphery of such materials in TEM images (Figure 3b and c), and bowl-shaped broken spheres in SEM images (Figure 3d and e) proved their hollow structure. It could also be observed from TEM image (Figure 3b) that those Fe_3O_4 hollow spheres were composed of some much smaller particles rather than formed by homogeneous Fe_3O_4 shells. Compared with other such uniformly walled structures, the nonsealed, somewhat loose nature of Fe_3O_4 hollow spheres facilitates their immobilization and subsequent encapsulation of various substances of biological and medical use in a similar way to that reported by Caruso et al.[25] Furthermore,

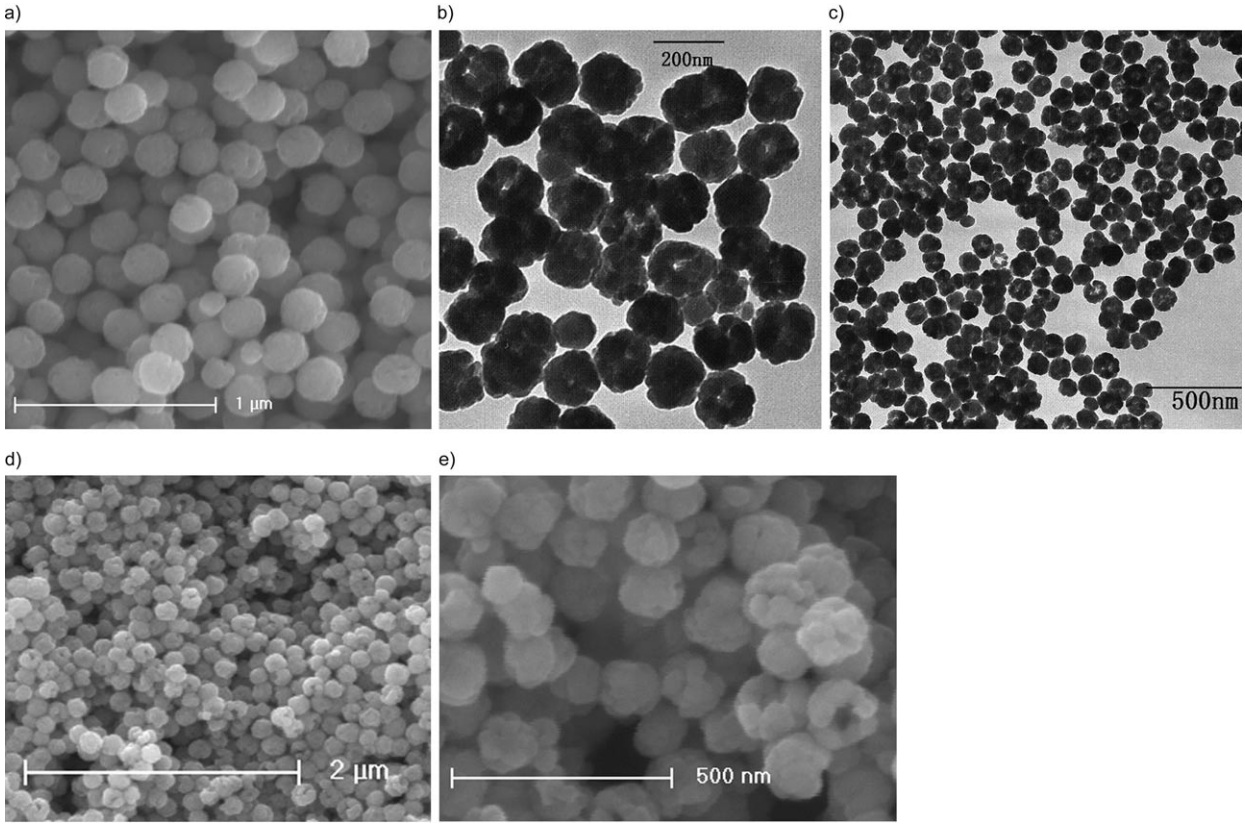

Figure 3. SEM images: a) ~200 nm Fe_3O_4 hollow nanospheres d,e) partly broken Fe_3O_4 hollow nanospheres. TEM images: b) ~150 nm Fe_3O_4 hollow nanospheres, c) ~100 nm Fe_3O_4 hollow nanospheres.

both SEM and TEM images demonstrated the narrow diameter distributions of such hollow nanospheres.

More detailed structural information of hollow Fe_3O_4 nanospheres was obtained by high-resolution TEM (HRTEM). Some representative HRTEM images of such hollow nanospheres are shown in Figure 4. The boxed area

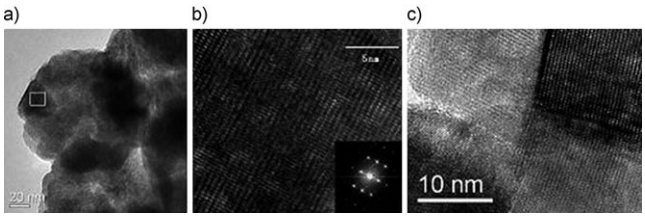

Figure 4. a) TEM image of ~120 nm hollow spheres; b) HRTEM image of the boxed region of image a) and its electron-diffraction pattern; c) HRTEM image of an interregional area that helps to explain the structure of hollow nanospheres.

in Figure 4a was further magnified to investigate its crystallinity. The regularly paralleled lattice fringes in Figure 4b indicate a single-crystal nature of the specific small particle in the selected area, while multidirection lattice fringes in one hollow sphere, shown in Figure 4c, ascertained the assumption that the agglomeration of plenty of small single-crystal particles leads to the formation of bulky hollow nanosphere.

The crystalline structure and phase purity were determined by powder X-ray diffraction (XRD) as shown in Figure 5. The positions and relative intensities of all diffraction peaks matched well with those from the JCPDS card (75–1610) for magnetite. The sharp, strong peaks confirmed

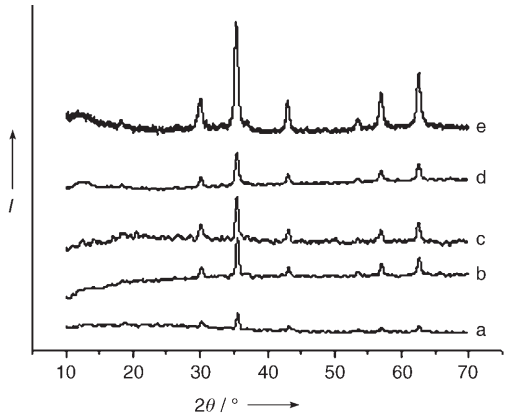

Figure 5. Powder X-ray diffractograms of the as-prepared magnetic nanoparticles of different size: a) ~15 nm, b) ~25 nm, c) ~35 nm, d) ~50 nm, and e) ~150 nm magnetic hollow nanospheres.

the products were well crystallized. So, the XRD results further revealed their high crystallinity.

To demonstrate their highly magnetic properties, the magnetic nanocrystals were studied by using a superconducting quantum interference device (SQUID) magnetometer at room temperature. The plots of magnetization versus magnetic field (M–H loop) at 25 °C for the typical magnetic nanoparticles and hollow nanospheres bound with 1,6-hexadiamine are illustrated in Figure 6. From the plots of M versus H, the saturation magnetization (M_s) was determined to be 41.3–59.8 emu g^{-1} for the amine-functionalized magnetite nanoparticles with tunable size from ~15 to ~50 nm. Meanwhile, the saturation magnetization of the ~150 nm hollow nanospheres reached 71.2 emu g^{-1}. Figure 6 displays the results of a study of the stability of aqueous solutions of amine-functionalized Fe_3O_4 nanocrystals and ordinary bare Fe_3O_4 particles; evidence was found that the Fe_3O_4 nanomaterials functionalized with aminoalkyl groups had much higher solubility and dispersibility than those of the unfunctionalized magnetite nanoparticles. From Figure 6j and f, it can be seen that the amine-functionalized magnetic nanoparticles can be dispersed in water to form a black solution. The nanoparticles can be drawn to the sidewall from the solution by applying a magnet besides the vial (Figure 6k). However, the unfunctionalized magnetic nanoparticles could not be easily dispersed in water and aggregated to the bottom of the vial within 5 min if the ultrasonication was stopped (see Figure 6g) and almost completely aggregated 20 min later (Figure 6i). The amine-functionalized magnetite nanomaterials, however, were stable and remained suspended in aqueous solution for more than one hour (Figure 6h). The good water solubility may result from the formation of hydrogen bonds between the amino groups and water. From the experimental results, it is clear that the amine-functionalized nanomaterials have highly magnetic properties and good water solubility, which makes them possible to be used in biotechnology and biomedicine.

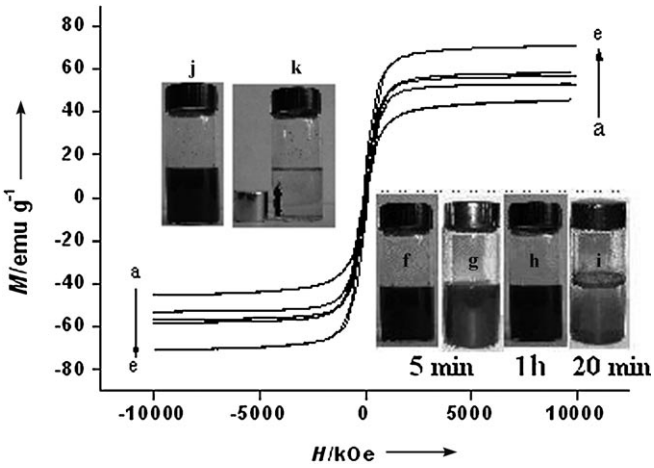

Figure 6. Room-temperature magnetization curves of obtained magnetite nanoparticles. a) ~15 nm, b) ~25 nm, c) ~35 nm, d) ~50 nm, and e) ~150 nm hollow nanospheres. The nanocrystals are easily dispersed in water (j) and also can be drawn from the solution to the sidewall of the vial by an assistant magnet field (k). With the ultrasonication, both the amine-functionalized (f, h) and nonfunctional magnetite nanocrystals were dispersed in water. After removing the ultrasonication, the nonfunctional magnetite nanocrystals began to aggregate within 5 min (g) and almost completely aggregated to the bottom of the vial within 20 min (i). However, the amine-functionalized magnetite nanocrystals did not aggregate, and even remained for more than one hour (h).

To provide direct proof for the amine functionalization, Fourier transform infrared (FTIR) spectroscopy was also used to characterize the amine-functionalized magnetite nanoparticles. Figure 7 shows the IR spectra of the amine-functionalized magnetic nanocrystals (Figure 7b) and the unfunctionalized magnetite nanoparticles (Figure 7a). The strong IR band at 567 cm^{-1} is characteristic of the Fe–O vibrations,[26] while the transmissions around 1626, 1485, and 874 cm^{-1} in Figure 7b from the amine-functionalized nanocrystals matched well with that from free 1,6-hexadiamine, indicating the existence of the free $-NH_2$ group on the amine-functionalized nanomaterials. No such bands were observed for the magnetic nanoparticles prepared in the absence of 1,6-hexadiamine (Figure 7a). The results from FTIR revealed that the magnetic nanocrystals have been functionalized with amino groups in the synthetic process.

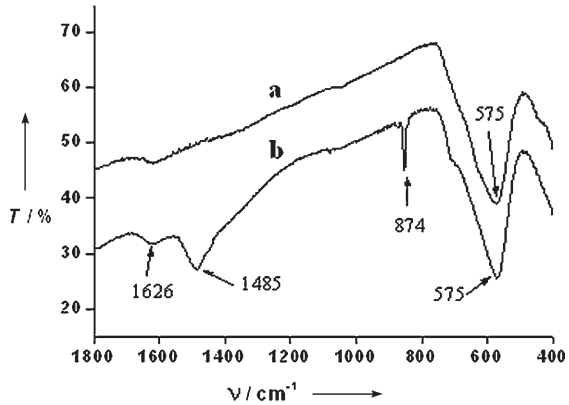

Figure 7. IR spectra of the a) unfunctionalized and b) amine-functionalized magnetite nanocrystals.

To demonstrate their potential of magnetic bioseparation and concentration in immunoassays, ~25 nm magnetite nanoparticles were bioconjugated with human immunoglobulin antigens (IgG-Ag) to form the antigen-labeled magnetic nanoparticle (MNP-Ag), and then used in the magnetic separation of fluorescein isothiocyanate (FITC)-labeled goat anti-human IgG antibodies (FITC-Ab1). The magnetic bioseparation process in the immunoassay is according to the scheme depicted in Figure 1. In this bioconjugating experiment, the antigens were attached to the surface of magnetic nanoparticles when activated carboxyl groups of the antigens and the amino groups on the nanoparticle surface formed covalent bonds.[27,28] Then the antigen-modified magnetic nanoparticles (MNP-Ag) were used in the magnetic

separation and concentration of FITC-Ab1. Based on the specific interaction between human IgG antigen and FITC-Ab1, FITC-Ab1 was concentrated and separated from the solution. Figure 8a shows the fluorescence spectra of both

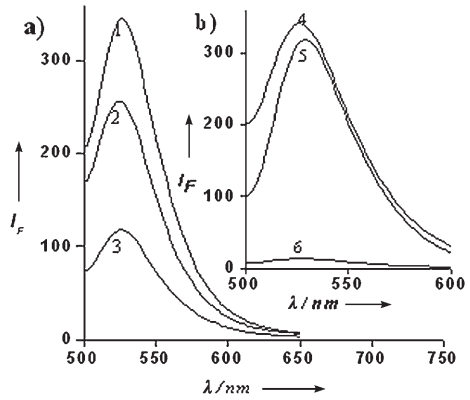

Figure 8. Fluorescence spectra of the immunoassay systems. a) Target experiment based on the human IgG antigen and FITC-Ab1 system; 1) FITC-labeled antibody solution; 2) MNP-Ag–Ab1-FITC solution; 3) supernatant solution after magnetic separation. b) Control experiment based on the human IgG antigen and FITC-Ab2 system; 4) FITC-Ab2 solution; 5) supernatant solution after magnetic separation; 6) MNP-Ag–ab2-FITC solution.

the MNP-Ag–Ab1-FITC nanocomposite solution (curve 2) and the supernatant after the magnetic separation (curve 3). From Figure 8a, it can be seen that the fluorescence of the supernatant is very weak; however, that of the nanocomposite solution is very strong, which means that FITC-Ab1 was bound to the magnetic nanoparticles and separated. The selectivity of the magnetic separation method has also been testified by the control experiment following a similar strategy (Figure 8b). In brief, the antibody used for magnetic bioseparation in the control experiment is FITC labeled goat anti-rabbit IgG antibody (FITC-Ab2) instead of the anti-human FITC-Ab1. The fluorescence intensity of the supernatant was virtually unchanged before (curve 4) and after (curve 5) the magnetic separation; meanwhile, the magnetic nanoparticle solution has no fluorescence (curve 6), which revealed that FITC-Ab2 was not bound to the human-IgG-antigen-modified magnetic nanoparticles. The results demonstrated the good selectivity of the present magnetic bioseparation technology based on the amine-functionalized magnetite nanoparticles, which also further verified the existence of the amino groups on the outer surface of the magnetic nanocrystals.

The exciting results of the in vitro application inspired us to test their in vivo potential. The in vivo potential applications were accomplished on MRI in live mice with ~25 nm amine-functionalized magnetic nanoparticles as a contrast agent. Figure S1 (in the Supporting Information) shows the imaging patterns from the live mice. It can be seen that the MRI signal decreases greatly from 293.52 (Figure S1a, before microinjection of magnetic nanoparticle) to 169.49 (Figure S1b, 30 min later); these results indicate that the nanoparticles have been phagocytosed by the liver macrophages. Our preliminary MRI experimental results indicated that the novel magnetite nanoparticles prepared by the current synthetic approach possess very good water solubility and highly magnetic properties, which makes them potentially useful as MRI contrast agents. It should be mentioned that the model mice removed from anaesthesia after the experiment and lived normally for more than a month. This, to some extent, demonstrated that the current sample has no acute fatal toxicity. Investigations into the biocompatibility and toxicity of the magnetic nanomaterials are currently in progress.

Conclusion

In summary, a facile one-pot strategy was put forward to prepare amine-functionalized magnetite nanoparticles and hollow nanospheres with excellent magnetism, tunable sizes, good monodispersibility, and crystallinity. These novel magnetite nanomaterials are water soluble because of their surface amino groups; hence the nanoparticles are easily dispersed in water and bioconjugated to biological macromolecules, such as peptides, proteins, and nucleic acids. Both the preliminary magnetic bioseparation in the immunoassay and the MRI experiment results revealed that the amine-functionalized magnetic nanocrystals prepared by this facile method possess very good magnetism and water solubility. We believe that these amine-functionalized magnetic nanocrystals can be used in fields such as magnetic bioseparation, immunoassay, MRI, and targeted drug delivery. With further development, the amine-functionalized hollow magnetite nanospheres may find excellent potentials in catalysis and targeted drug delivery.

Experimental Section

Chemicals: All chemicals were analytical grade and used as received without further purification. Deionized water was used throughout. Human immunoglobulin antigen and fluorescein isothiocyanate (FITC) labeled antibodies were purchased from Century Forlin-Biotechnology Co. Ltd, Beijing, China. 1-Ethyl-3-(3-dimethlyaminopropyl)carbodiimide (EDAC, Sigma) and *N*-hydroxysuccinimide (NHS, Acros) were used for immunoassays. Other chemicals were all supplied by the Beijing Chemical Reagent Company.

Preparation of amine-functionalized magnetic nanoparticles: In the case of ~25 nm magnetic nanoparticles, a solution of 1,6-hexanediamine (6.5 g), anhydrous sodium acetate (2.0 g) and $FeCl_3{\cdot}6H_2O$ (1.0 g) as a ferric source[24,29] in glycol (30 mL) was stirred vigorously at 50 °C to give a transparent solution. This solution was then transferred into a Teflon-lined autoclave and reacted at 198 °C for 6 h. The magnetite nanoparticles were then rinsed with water and ethanol (2 or 3 times) to effectively remove the solvent and unbound 1,6-hexanediamine, and then dried at 50 °C before characterization and application. During each rinsing step, the nanoparticles were separated from the supernatant by using magnetic force. For other size particles, the experiment procedures are similar except that the amount of the 1,6-hexanediamine was increased from 5.0 to 7.0 mL, the solvothermal temperature increased from 190 to 205 °C,

and the particle size decreased from ~50 to ~15 nm. Although the temperature and amount of 1,6-hexanediamine greatly influenced the particle size, the effects were not linear owing to the complex nature of the growth process. Moreover, prolonging the reaction time had no evident influence on the particle size. As shown by experiments that we repeated many times, no single-crystal Fe_3O_4 nanoparticles larger than 50 nm in diameter were synthesized in the presence of 1,6-hexadiamine.

Preparation of amine-functionalized magnetic hollow nanospheres: Control experiments showed that adjusting 1,6-hexadiamine to a lower concentration and increasing the amount of anhydrous sodium acetate lead to the preparation of hollow nanospheres. For example, the magnetite hollow nanospheres of ~100 nm were prepared by dissolving $FeCl_3{\cdot}6H_2O$ (1.0 g) in ethylene glycol (30 mL), and then anhydrous sodium acetate (4.0 g) and 1,6-hexadiamine (3.6 g) were added and stirred vigorously to acquire a transparent solution. The mixture was sealed in a Teflon-lined stainless-steel autoclave and was heated at 200 °C for 6 h. The product, which settled at the bottom of the autoclave, was washed with hot water and ethanol (3 times) under ultrasonic conditions to remove the solvent and unbound 1,6-hexanediamine effectively, and then dried at 50 °C to gain the black powder. The product was separated from various solvents by using magnetic force during each step. Hollow nanospheres of different sizes (100–200 nm) were prepared by changing the quantity of $FeCl_3{\cdot}6H_2O$ from 0.4 to 1.0 g and the temperature from 190 to 205 °C.

Bioconjugation of magnetic nanoparticles with IgG-Ag: The method for the human IgG-Ag bioconjugation to the magnetite nanoparticles was similar to that of the reported protocols.[27,28] Briefly, ~25 nm amine-functionalized magnetic nanoparticles (5 mg) was dispersed in phosphate-buffered saline (PBS, Na_2HPO_4 8.0 mM, NaH_2PO_4 2 mM, NaCl 0.15 M, Tween 20 0.05 %, pH 7.4; 5.0 mL) by ultrasound irradiation technology, followed by addition of human immunoglobulin antigen (IgG-Ag; 0.1 mmol) with stirring. Then 1-ethyl-3-(3-dimethlyaminopropyl)carbodiimide (EDAC; 0.1 mmol) and *N*-hydroxysuccinimide (NHS; 0.2 mmol) were added. The reaction mixture was stirred at room temperature under N_2 for 4 h. Excess IgG-Ag, EDAC, and NHS were removed by magnetic field separation and rinsed with PBS solution (three times). The Ag-modified magnetic nanoparticles were redispersed in PBS (5.0 mL) and stored at 4 °C for use.

Magnetic separation of target antibody: The antigen-modified magnetic nanoparticles were used in the magnetic separation and concentration of the target fluorescein isothiocyanate (FITC)-labeled goat anti-human IgG antibody (FITC-Ab1). In a typical experiment, a solution antigen-modified magnetite nanoparticle in PBS (MNP-Ag, 100 μL, 1 mg mL^{-1}) was added to a solution of FITC-Ab1 in water (200 μL 2 mg mL^{-1}) with stirring and the mixture was incubated at room temperature for 2 h. The mixture was then thoroughly mixed and the fluorescence of the mixed solution was recorded immediately before magnetic separation. The MNP-Ag–Ab-FITC composite was separated by magnetic-field separation technology and washed with PBS buffer solution (3 times). The fluorescence of the nanocomposite solution and the supernatant were measured. The selectivity of this magnetic separation method was accomplished by the control experiment following the same procedure described in the target experiment.

In vivo magnetic resonance imaging: The in vivo magnetic resonance imaging experiments were accomplished by intravenous microinjection of the magnetite microfluid at a dose of 0.02 μmol kg^{-1} of body weight into a tail trail vein of the live mice, before which the mice were anesthetized by intraperitoneal injection of ketamine/xylazine hydrochloride (1:1) at a dose of 1 mg kg^{-1} of body weight. Then magnetic resonance imaging experiments were performed.

Characterization: The TEM images were taken using a H-800 (Hitachi, Japan) transmission electron microscope with a tungsten filament at an accelerating voltage of 200 kV. Samples were prepared by placing a drop of a dilute alcoholic dispersion of nanocrystals on the surface of a copper grid. Electron diffraction was also performed to study the single-crystal nature of the samples on a high-resolution transmission electron microscope (HRTEM, JEM-200CX). The JSM-6301F scanning electron microscope was applied to acquire the SEM image of the Fe_3O_4 hollow nanospheres. XRD measurement was performed on a Bruker D8 Advance X-ray diffractometer by using $Cu_{K\alpha}$ radiation ($\lambda = 0.15418$ Å). The operation voltage and current were kept at 40 kV and 40 mA, respectively. The 2θ range used in the measurement of Fe_3O_4 nanoparticles was 10–70° in steps of 0.02° with a count time of 1 s. A superconducting quantum interference device (SQUID) magnetometer (LakeShore 7307) was used in the magnetic measurement. Fluorescence spectra were carried out on an F-4500 fluorescence spectrophotometer (Hitachi, Japan). FTIR spectra were conducted with a Nicolet 560 Fourier-transform infrared spectrophotometer. MRI images were acquired using a GE VH/i^{TM} 3.0T (GE, USA) magnetic resonance imaging device.

Acknowledgements

This work was supported by NSFC (90406003, 50372030, 20131030, 20401010), the Specialized Research Fund for the Doctoral Program of Higher Education, the Foundation for the Author of National Excellent Doctoral Dissertation of P. R. China and the State Key Project of Fundamental Research for Nanomaterials and Nanostructures (2003CB716901).

[1] a) W. C. W. Chan, S. Nie, *Science* **1998**, *281*, 2016–2018; b) M. Bruchez, D. J. Moronne, P. Gin, S. Weiss, A. P. Alivisatos, *Science* **1998**, *281*, 2013–2016; c) D. B. Robinson, H. H. J. Persson, H. Zeng, G. X. Li, N. Pourmand, S. H. Sun, S. X. Wang, *Langmuir* **2005**, *21*, 3096–3103; d) S. G. Grancharov, H. Zeng, S. H. Sun, S. X. Wang, S. O'Brien, C. B. Murray, J. R. Kirtley, G. A. Held, *J. Phys. Chem. B* **2005**, *109*, 13030–13035.

[2] C. Xu, K. Xu, H. Gu, X. Zhong, Z. Guo, R. Zheng, X. Zhang, B. Xu, *J. Am. Chem. Soc.* **2004**, *126*, 3392–3393.

[3] A. Dyal, K. Loos, M. Noto, S. W. Chang, C. Spagnoli, K. V. P. M. Shafi, A. Ulman, M. Cowman, R. A. Gross, *J. Am. Chem. Soc.* **2003**, *125*, 1684–1685.

[4] T. Mirzabekov, H. Kontos, M. Farzan, W. Marasco, J. Sodroski, *Nat. Biotechnol.* **2000**, *18*, 649–654; D. Cao, P. He, N. Hu, *Analyst* **2003**, *128*, 1268–1274.

[5] a) P. S. Doyle, J. Bibette, A. Bancaud, J. Viovy, *Science* **2002**, *295*, 2237; b) S. I. Stoeva, F. W. Huo, J. S. Lee, C. A. Mirkin, *J. Am. Chem. Soc.* **2005**, *127*, 15362–15363.

[6] H. Gu, P. Ho, K. W. T. Tsang, L. Wang, B. Xu, *J. Am. Chem. Soc.* **2003**, *125*, 15702–15703.

[7] D. Wang, J. He, N. Rosenzweig, Z. Rosenzweig, *Nano Lett.* **2004**, *4*, 409–413.

[8] a) J. Won, M. Kim, Y. W. Yi, Y. H. Kim, N. Jung, T. K. Kim, *Science* **2005**, *309*, 121–125; b) H. H. Yang, S. Q. Zhang, X. L. Chen, Z. X. Zhuang, J. G. Xu, X. R. Wang, *Anal. Chem.* **2004**, *76*, 1316–1321; c) Y. Deng, C. Wang, X. Shen, W. Yang, L. Jin, H. Gao, S. Fu, *Chem. Eur. J.* **2005**, *11*, 6006–6013.

[9] T. J. Yoon, J. S. Kim, B. G. Kim, K. N. Yu, M. H. Cho, J. K. Lee, *Angew. Chem.* **2005**, *117*, 1092–1095; *Angew. Chem. Int. Ed.* **2005**, *44*, 1068–1071.

[10] J. M. Perez, L. Josephson, T. O'Loughlin, D. Högemann, R. Weissleder, *Nat. Biotechnol.* **2002**, *20*, 816–820.

[11] J. M. Perez, T. O'Loughlin, F. J. Simeone, R. Weissleber, L. Josephson, *J. Am. Chem. Soc.* **2002**, *124*, 2856–2857.

[12] J. M. Nam, C. S. Thaxton, C. A. Mirkin, *Science* **2003**, *301*, 1884–1886.

[13] I. Willner, E. Katz, *Angew. Chem.* **2003**, *115*, 4724–4737; *Angew. Chem. Int. Ed.* **2003**, *42*, 4576–4588.

[14] M. Zhao, M. F. Kircher, L. Josephson, R. Weissleder, *Bioconjugate Chem.* **2002**, *13*, 840–844.

[15] D. Hogemann, V. Ntziachristos, L. Josephson, R. Weissleder, *Bioconjugate Chem.* **2002**, *13*, 116–121.

[16] a) D. K. Yi, S. T. Selvan, S. S. Lee, G. C. Papaefthymiou, D. Kundaliya, J. Y. Ying, *J. Am. Chem. Soc.* **2005**, *127*, 4990–4991; b) Y. Lee, J. Lee, C. J. Bae, J. Park, H. Noh, J. H. Park, T. Hyeon, *Adv. Funct. Mater.* **2005**, *15*, 503–509.

[17] L. A. Harris, J. D. Goff, A. Y. Carmichael, J. S. Riffle, J. J. Harburn, T. G. S. Pierre, M. Saunders, *Chem. Mater.* **2003**, *15*, 1367–1377.
[18] V. G. Pol, M. Motiei, A. Gedanken, J. Calderon-Moreno, Y. Mastai, *Chem. Mater.* **2003**, *15*, 1378–1384.
[19] a) X. W. Teng, H. Yang, *J. Am. Chem. Soc.* **2003**, *125*, 14559–14563; b) T. Hyeon, S. S. Lee, J. Park, Y. Chung, H. B. Na, *J. Am. Chem. Soc.* **2001**, *123*, 12798–12801.
[20] H. Zeng, P. M. Rice, S. X. Wang, S. H. Sun, *J. Am. Chem. Soc.* **2004**, *126*, 11458–11459.
[21] S. H. Sun, H. Zeng, D. B. Robinson, S. Raoux, P. M. Rice, S. X. Wang, G. X. Li, *J. Am. Chem. Soc.* **2004**, *126*, 273–279.
[22] J. Rockenberger, E. C. Scher, P. A. Alivisatos, *J. Am. Chem. Soc.* **1999**, *121*, 11595–11596.
[23] J. Park, K. An, Y. Hwang, J. G. Park, H. J. Noh, J. Y. Kim, J. H. Park, N. M. Hwang, T. Hyeon, *Nat. Mater.* **2004**, *3*, 891–893.
[24] H. Deng, X. L. Li, Q. Peng, X. Wang, J. P. Chen, Y. D. Li, *Angew. Chem.* **2005**, *117*, 2842–2845; *Angew. Chem. Int. Ed.* **2005**, *44*, 2782–2785.
[25] Y. Wang, F. Caruso, *Chem. Mater.* **2005**, *17*, 953 –961.
[26] I. J. Bruce, J. Taylor, M. Todd, M. J. Davies, E. Borioni, C. Sangregorio, T. Sen, *J. Magn. Magn. Mater.* **2004**, *284*, 145–160.
[27] W. Yang, C. G. Zhang, H. Y. Qu, H. H. Yang, J. G. Xu, *Anal. Chim. Acta* **2004**, *503*, 163–169.
[28] H. J. Kim, W. L. Shekver, Q. X. Li, *Anal. Chim. Acta* **2004**, *509*, 111–118.
[29] Z. Li, Q. Sun, M. Y. Gao, *Angew. Chem.* **2004**, *116*, 125–128; *Angew. Chem. Int. Ed.* **2005**, *44*, 123–126.

Received: October 27, 2005
Revised: February 17, 2006
Published online: June 1, 2006

